ADVANCED OPTICAL MATERIALS
www.advopticalmat.de

# Rationalizing the Amplified Spontaneous Emission Mechanism in $CsPbBr_3$ Perovskite Nanocrystals Films by means of Optical Gain Measurements

*Stefania Milanese, Maria Luisa De Giorgi, Marco Anni, Maryna I. Bodnarchuk, and Luis Cerdán**

**With their exceptional optoelectronic properties, $CsPbBr_3$ perovskite nanocrystals (NCs) are promising materials for light-emitting devices. Elucidating their stimulated emission mechanisms is fundamental to grasp the limitations hindering their use as electrically pumped lasers. In particular, two questions remain open: why the Amplified Spontaneous Emission (ASE) band is significantly shifted from the fluorescence one, and why the former seems to suddenly emerge from, and coexist with, the latter. Here, these questions are addressed through experimental ASE measurements, combined with numerical simulations and a comprehensive assessment of the performance of different analytical expressions used in the literature to retrieve the optical gain from these experiments. This multi-facet study shows that the ASE behavior in $CsPbBr_3$ NCs thin films stems from four distinctive processes: reabsorption due to a large overlap between the absorption and fluorescence spectra, a strong contribution of excited state absorption within the fluorescence window, the excitation of differently polarized waveguide modes, and the coexistence of short- and long-lived localized excitons. The results in this work delineate the best practices to analyze the optical gain in perovskite samples, help to understand their ASE mechanisms, and provide insights to boost their lasing efficiency.**

## 1. Introduction

Thanks to their optical and electronic properties, lead halide perovskites –with the general formula $APbX_3$, with A a cation and X a halogen anion ($I^-$, $Br^-$, or $Cl^-$)– have become prominent materials to implement photonic and optoelectronic devices,[1,2] including solar cells,[3,4] nonlinear optical devices,[5] photodetectors,[6,7] light emitting diodes,[8,9] and lasers.[10–13] The synthesis of these materials as colloidal nanocrystals (NCs) or quantum dots has boosted their applicability further. First, because of their facile and low-cost production, and their ease of processing, they result highly attractive from a commercial point of view.[14] And second, because the quantum confinement effects arising from their nanoscale nature lead to bright and narrow fluorescence bands with excellent photoluminescence quantum yields (PLQY).[15,16] Furthermore, their bandgap and, with it, the absorption and emission spectral position, can be swiftly tuned from the UV down to the IR by changing the size, shape, and composition of the NCs.[17,18]

A few months after their first synthesis,[17] low threshold Amplified Spontaneous Emission (ASE) and lasing at room temperature were demonstrated in $CsPbX_3$ NCs thin films, both under femtosecond[19] and nanosecond[20] pulsed excitation. In addition, full ASE color tuning across the entire visible spectrum was achieved by compositional modulation and size control,[20] opening the way for the employment of fully inorganic perovskite NCs as photonic sources. The demonstration of high gain and low ASE threshold in $CsPbBr_3$ NCs thin films[21–26] further stimulated the research toward the implementation of fully inorganic perovskite NCs as active materials for lasing with different cavity geometries, such as Vertical Cavity Surface Emitting Lasers,[27–30] Whispering Gallery Modes,[31–34] and Distributed Feedback Lasers.[35,36] Understanding the origin and

S. Milanese, M. L. De Giorgi, M. Anni
Dipartimento di Matematica e Fisica "Ennio De Giorgi"
Università del Salento
Via per Arnesano, Lecce 73100, Italy

The ORCID identification number(s) for the author(s) of this article can be found under https://doi.org/10.1002/adom.202401078



**DOI: 10.1002/adom.202401078**

M. I. Bodnarchuk
Institute of Inorganic Chemistry
Department of Chemistry and Applied Bioscience
ETH Zürich, Zürich CH-8093, Switzerland

M. I. Bodnarchuk
Laboratory for Thin Films and Photovoltaics
Empa – Swiss Federal Laboratories for Materials Science and Technology
Dübendorf CH-8600, Switzerland

L. Cerdán
Instituto de Química Física "Blas Cabrera"
Consejo Superior de Investigaciones Científicas
Madrid 28006, Spain
E-mail: l.cerdan@csic.es

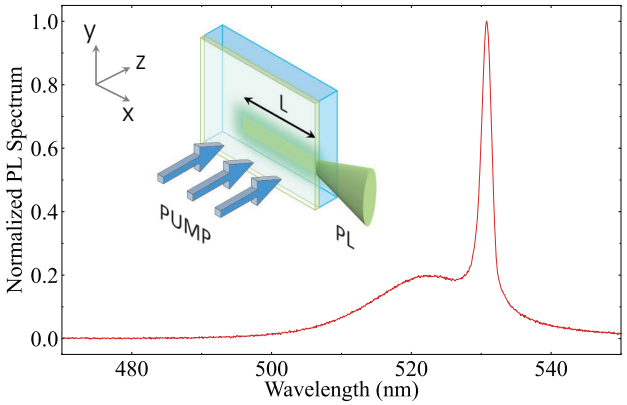


**Figure 1.** Experimental waveguided PL spectrum for sample NC-DDAB at a pump fluence of 1.3 mJ cm$^{-2}$ and a stripe length $L$ = 0.45 cm. Inset: Schematics of a typical experimental configuration to measure ASE in thin films, where the excitation stripe, of length $L$, impinges normal to the film ($z$-axis), and the PL propagating along the $x$-axis is collected by a spectrometer.

mechanisms of their stimulated emission signatures and properties is fundamental to address their possible limitations and to achieve much more efficient perovskite lasers, with the ultimate goal of attaining continuous wave excitation[10,12] and/or electrical excitation.[37]

$CsPbBr_3$ NCs, and most perovskites for that matter, display very distinctive ASE spectral signatures.[13,19,20,38,39] In conventional organic materials –such as dyes, oligomers, or polymers–, when the excitation density is increased, the photoluminescence (PL) spectrum gradually narrows down from a fluorescence spectrum to a well-resolved ASE band whose peak is close to the fluorescence one.[40] In perovskite NCs, in contrast, the ASE band is usually significantly shifted from the fluorescence one, and, in addition, the former seems to suddenly emerge from, and coexist with, the latter. In other words, the PL spectrum is seemingly comprised of a strong background fluorescence signal, and a well-resolved, shifted ASE band, as we exemplify in **Figure 1**. These features have led to a debate, which is not settled yet, on which is the mechanism behind the ASE band shift. Based on the accumulated knowledge on colloidal semiconductor NCs and quantum dots,[41] the ASE band was initially ascribed to either excitons[20] or biexcitons.[19] In the latter case, the shift owed to the energy invested in dissociating the biexcitons (binding energy ≈50 meV) during its recombination. In the single exciton scenario, in contrast, it was observed that the ASE peak overlaps with the edge of the absorption band (Urbach tail), and thus the redshift would come from reabsorption, i.e., the longpass filtering effect that the ground state absorption has on the PL. More recently, it has been settled that, while different emissive states can be excited –free excitons,[42–45] localized excitons bound to surface states,[42,43] biexcitons,[44,46–48] and even trions (charged excitons)[44,49]–, at room temperature, and mild excitation densities, the emission is dominated by localized excitons.[42,47,50,51] Hence, there is currently a partial consensus in that the ASE physical mechanism in $CsPbBr_3$ NCs films can be rationalized as coming from localized excitons, inhomogeneously broadened due to the NCs size dispersion, subject to light reabsorption.[47,50,52,53]

Nevertheless, two facts suggest that reabsorption cannot fully account for the experimental observations. First, the redshifts due to reabsorption affect similarly ASE and fluorescence (as shown in the Experimental Section of this manuscript), meaning that there shouldn't be such a large detuning between them. In this sense, a recent work on $CsPbBr_3$ NCs films reported simulation results, assuming reabsorption and inhomogeneous broadening as the effective mechanisms responsible for ASE, and showed that the ASE and background fluorescence bands are barely detuned.[50] Second, the analytical expressions used to retrieve the optical gain in this kind of devices, like the ones used for the Variable Stripe Length (VSL) method,[54] implicitly account for reabsorption effects, but they usually fail in fitting the experimental results. In fact, an alternative expression, initially intended to account for the presence of both excitons and biexcitons in emission,[55] has been shown to fit better to the VSL data in perovskite samples,[19,56] suggesting the contribution of different emitters to the total emission. Accordingly, the mechanisms behind the PL spectral signatures in $CsPbBr_3$ NCs have yet to be fully elucidated.

Here, we focus on the rationalization of the PL properties and spectral signatures of $CsPbBr_3$ NCs films by means of experimental ASE optical gain measurements, guided by numerical results and analytical assessments. In particular, our aim is to answer why the ASE band peak is significantly shifted from the fluorescence maximum, and, also, why the former seems to suddenly emerge from, and coexist with, the latter. As we rely on ASE gain measurements to tackle this problem, in the first part of the manuscript we carry out a comprehensive study of the performance –against $CsPbBr_3$ NCs thin films data– of different analytical expressions used in the literature to retrieve the optical gain from ASE experiments. We conclude that only those accounting for two signals (ASE plus background fluorescence) and gain saturation are satisfactory. Finally, using this thorough analysis, together with polarization resolved ASE experiments and time-resolved numerical simulations, we ascribe both the shifted ASE band and the excess fluorescence background not only to reabsorption, but also to excited state absorption and a coexistence of short- and long-lived localized excitons. The results in this work delineate the best practices to analyze the optical gain in perovskite samples, help to understand the mechanisms behind the PL signatures of $CsPbBr_3$ NCs, and other perovskites in general, and provide insightful information on how to boost the efficiency of perovskite lasers.

## 2. Results and Discussion

We show in the inset of Figure 1 the prototypical pump/detection configuration to study the ASE properties in waveguides. In it, the sample, placed in the $xy$-plane, is excited by a laser beam propagating along the $z$-axis, with a spot shaped as a rectangular stripe with length much longer than its width, and whose end is placed right up to the edge of the sample. The generated PL emission, which is preferentially amplified in the direction set by the stripe, is collected along the $x$-axis. The PL emission is acquired either as a function of the pump excitation density, typically to retrieve the ASE threshold, or as a function of the stripe length, to estimate the optical gain, as explained in the Experimental Section.

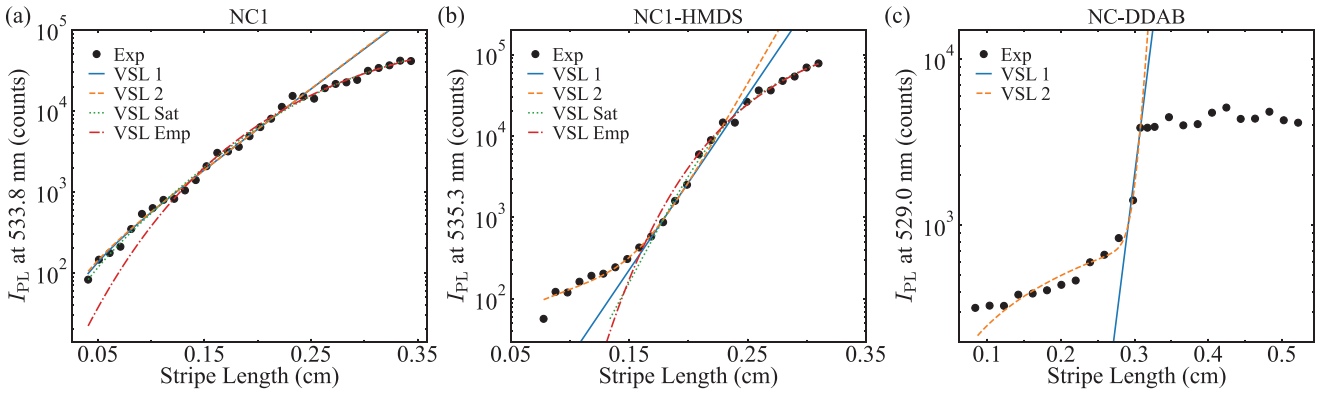


**Figure 2.** VSL method analysis: VSL experimental data (black points) and best fits (colored lines) for the different VSL expressions used in this manuscript (see text for details) for: a) sample NC1 at a pump fluence of 1.5 mJ $cm^{-2}$, b) sample NC1-HMDS at a pump fluence of 2.1 mJ $cm^{-2}$ and c) sample NC-DDAB at a pump fluence of 2.4 mJ $cm^{-2}$. All the gain measurements have been performed at pump densities about 2-2.5 times above the ASE threshold.

### 2.1. VSL Analysis

We have plotted in **Figure 2** examples of ASE measurements (black points), using the VSL method, for three different thin film samples based on $CsPbBr_3$ NCs. For those interested readers, we have included in Table S1 (Supporting Information) a collection of spectroscopic, ASE, and optical gain properties of these samples. In addition, we have added in Figure S1 (Supporting Information) their losses' coefficient spectra together with fluorescence microscope maps to assess the quality of the films. These examples are representative of the typical trends observed for this kind of material. Sample NC1 in Figure 2a displays a nearly exponential growth at the whole range of stripe lengths. Sample NC1-HMDS in Figure 2b, shows this trend at mid and long stripe lengths, but it displays a subexponential growth at the shortest ones. The PL in sample NC-DDAB, Figure 2c, grows subexponentially at the shortest stripe lengths, shows a nearly exponential increase at mid-stripe lengths but, at the longest stripe lengths, it suddenly saturates to a nearly constant value, as already observed previously by other authors.[57–59]

As we explain in the Experimental Section, the optical gain value, *g*, is obtained by fitting the adequate mathematical expression to these data. We have included in Figure 2 the best fits of the VSL expressions considered in this work. For expressions VSL 1, Equation (1), and VSL 2, Equation (2), in sample NC1 we have to exclude from the fit the longest stripe lengths, as there are clear signatures of gain saturation (Figure 2a). Both expressions fit well to the data, and give almost the same results with gain values of $g = 22.7 \pm 0.7$ $cm^{-1}$ and $g = 23.0 \pm 2.1$ $cm^{-1}$, respectively. At the same time, the proportionality factors in expression VSL 2, Equation (2), fulfill $A_1 \gg A_2$, suggesting that there is no obvious presence of two emitting species, or signals for that matter. The clear presence of gain saturation calls for the use of VSL expressions accounting for this effect. Expression VSL Sat, Equation (3), fits almost perfectly to the experimental data at all stripe lengths, yielding an optical gain of $g = 26.5 \pm 1.1$ $cm^{-1}$. This *g* value is quite in agreement with the values obtained with VSL 1 and VSL 2. On the other hand, expression VSL Emp, Equation (5), fits rather well the longest stripe lengths, but fails at the shortest. In addition, it heavily overestimates the gain as compared with the other VSL expressions, yielding values of $g = 76$ $cm^{-1}$, with a quite significant error of $\pm 20$ $cm^{-1}$, as previously observed by other authors.[57,60]

Sample NC1-HMDS shows a slightly different behavior (Figure 2b). For VSL 1 we must exclude from the fit not only the longest stripes, due to gain saturation, but the shortest ones as well, due to a clear background signal. Under these conditions, VSL 1 gives an optical gain value of $g = 49.7 \pm 2.4$ $cm^{-1}$. In contrast, for VSL 2 there is no need to remove the shortest stripes, as the excess PL intensity in this range is accounted for by Equation (2). Thus, VSL 2 fits quite well to the experimental data and yields an optical gain of $g = 57.6 \pm 2.4$ $cm^{-1}$. Obviously, this result indicates the excitation of two independent contributions to the PL signal, the origin of which will be elucidated along the following pages. On the other hand, for expressions VSL Sat and VSL Emp we must exclude the shortest stripes from the fit but, even though, the fits are not fully satisfactory. VSL Sat fits just well to the chosen points, and gives an optical gain that is slightly larger than that of VSL 2 and with a larger error ($g = 63.3 \pm 5.0$ $cm^{-1}$). VSL Emp, in contrast, fits only the largest stripes and gives, again, a heavily overestimated and uncertain optical gain ($g = 460 \pm 240$ $cm^{-1}$).

Sample NC-DDAB is the most challenging sample in terms of VSL expressions fitting, as we show in Figure 2c. For VSL 1 we must only use three points at $L \approx 0.3$ cm to avoid the gain saturation and signal background regions, and, thus, to have a proper fit. This translates into a huge uncertainty in the fitted optical gain ($g = 81 \pm 29$ $cm^{-1}$). For VSL 2 we can use more data, but the fit is still not highly satisfactory. Anyhow, this model yields a larger optical gain and a smaller error ($g = 147.0 \pm 8.4$ $cm^{-1}$), and points to the excitation of two independent signals in this sample. Finally, we tried to fit VSL Sat and VSL Emp to the data, but the algorithm did not yield a reliable solution. This unsuccessful attempt suggests that the observed plateau in the PL intensity cannot be simply explained by a conventional gain saturation process –excited state population depletion– but, rather, by extrinsic factors, such as a film thickness inhomogeneity. Incidentally, these gain values are comparable to those obtained in similar experimental conditions, both for NCs[61] and bulk perovskite films.[62,63]

**Table 1.** Applicability conditions and limitations of the different gain analysis methods assessed in this manuscript.

| Expression | Saturation | Two Signals | Intuitive | Usage | Physical Model |
|---|---|---|---|---|---|
| VSL 1 [Equation (1)] | no | no | yes | easy | yes |
| VSL 2 [Equation (2)] | no | yes | yes | easy | yes |
| VSL Sat [Equation (3)] | yes | no | moderately | moderate | yes |
| VSL Emp [Equation (5)] | yes | no | moderately | easy | no |
| VPI 1 [Equation (6)] | yes | no | yes | moderate | yes |
| VPI 2 [Equation (8)] | yes | yes | yes | moderate | yes |

These results provide guidelines to choose a method to measure optical gains from VSL experiments, specially in perovskite samples. We present in **Table 1** some applicability conditions that we considered that should be fulfilled to choose the best analytical methodology. We have based these criteria on the capability of the VSL expression to capture experimental trends (saturation and/or two signals), on some practical aspects (to be intuitive and easy to use/implement), as well as on fundamental aspects such as the existence of a physical model from which to derive the analytical expression, which is always desirable in Physics. From the information in Table 1, and the results in Figure 2, we can conclude the following:

1. None of the proposed VSL models ticks all the boxes and, hence, one must always ensure that the data chosen for the fitting procedure comply with the assumptions behind the analytical expression.
2. We do not recommend the use of the empirical expression VSL Emp, Equation (5), as it cannot fit properly the shortest stripes, even when there is just a single signal, and it is not backed up by any physical model. In addition, it tends to heavily overestimate the optical gain values.
3. Whenever possible, we recommend to use directly expression VSL Sat, as it is not difficult to implement, is backed-up by a physical model, and works rather well both when there is a moderate gain saturation and in the absence of it (small-signal regime). Although, if the fitted curve underestimates the PL intensity at the shortest stripe lengths, it could mean that there is a contribution of a background signal. In such cases, one should use instead expression VSL 2 only for the shortest stripe lengths to avoid gain saturation.

### 2.2. VPI Analysis

In the Variable Pump Intensity (VPI) method, the PL signal is acquired as a function of the pump excitation density, typically to retrieve the ASE threshold and peak wavelength. The interested reader can find in Figure S2 (Supporting Information) the VPI spectrographs corresponding to the three samples analyzed in this work, where it becomes clear that ASE wavelength barely changes within the pump fluence range used for these experiments. As explained in the Experimental Section, we have recently proposed a new methodology (expression VPI 1, Equations (6) and (7), in this manuscript) that allows to retrieve the optical gain from the VPI method PL spectra.[64] In this section, we will compare the results obtained with expression VPI 1 with those yielded by VPI 2, Equation (8), that we are introducing in this work. We implemented the modified version VPI 2 in view of the necessity of accounting for two signals (ASE plus background fluorescence) that came up when calculating the optical gain with the VSL method.

For the sake of brevity, we will focus in the main text on the results of sample NC-DDAB (**Figure 3**), but the analysis and conclusions drawn from this sample can be directly extrapolated to samples NC1 and NC1-HMDS (Figures S3 and S4, Supporting Information). First, we observe that both VPI 1 and VPI 2 allow obtaining a very accurate fit of the emission spectrum above the ASE threshold (see Figure 3a) even when VPI 1 assumes that the whole PL emission comes from ASE (solid blue line) while, according to VPI 2, the acquired PL spectrum is the combination of a strong fluorescence background (dotted red line) and a distinctive ASE band (dashed red line). Concerning the emission intensity, we have plotted in Figure 3b the experimental PL signal (green points) at 530.8 nm –the ASE peak wavelength– as a function of the pump fluence. At a certain threshold pump fluence (≈0.65 mJ $cm^{-2}$), it shows the change in slope characteristic of the onset of ASE. This change in slope is accompanied by a reduction in the Full Width Half Maximum (FWHM) due to the preferential amplification of the wavelengths nearer to the gain maximum (Figure 3c). In most publications, these two plots, together with the visual estimation of the threshold position, suffice to conclude that the sample displays ASE and, by extension, optical gain.

The experimental pump fluence dependence of the emission intensity (Figure 3b) can be excellently reproduced by the best fits of both expressions VPI 1 (solid blue line) and VPI 2 (solid red line). However, we observe that, even if the goodness of fit of expression VPI 1 could suggest the presence of only one signal, the results from VPI 2 suggest otherwise, in agreement with the VSL analysis of Figure 2c. Indeed, below ASE threshold the PL signal is dominated by a background fluorescence contribution (dotted red line) that grows linearly with the pump fluence, in accordance with its non-amplified nature. It is only when approaching threshold that a strong purely ASE signal (dashed red line) becomes noticeable and surpasses the fluorescence background. This is in agreement with the experimental observation that, for perovskites in general, the PL spectrum does not narrow down gradually from a fluorescence spectrum to an ASE band but, rather, the latter seems to suddenly emerge from, and coexist with, the former. Actually, this sense of emergence can be clearly visualized in Figure 3a, strongly suggesting the presence of two contributions to the total emission.

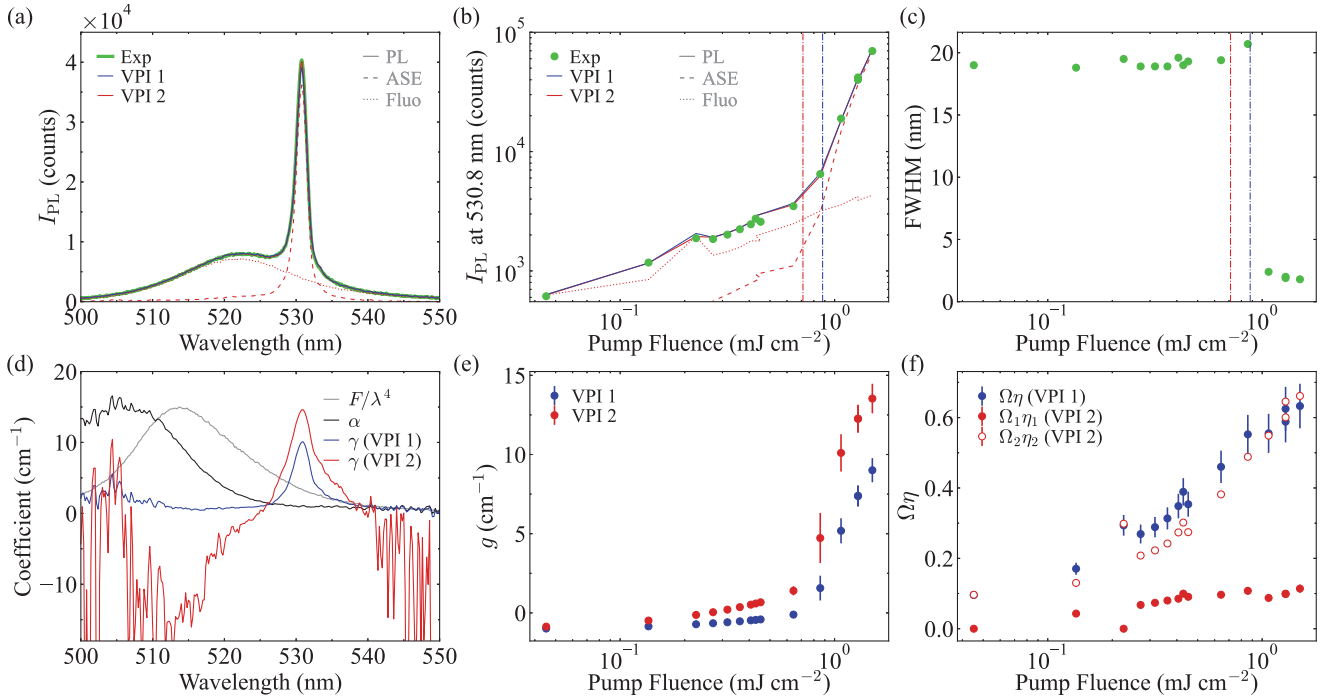


**Figure 3.** VPI method analysis for sample NC-DDAB: a) Experimental PL spectrum (thick solid green line) at a pump fluence of 1.3 mJ cm$^{-2}$, and best fits for the models VPI 1 (solid blue line, Equation (6)) and VPI 2 (solid red line, Equation (8)). The dashed and dotted red lines show the contributions of pure ASE and background fluorescence, respectively. We will follow the same color code in the remaining panels. b) Experimental PL intensity at peak wavelength versus pump fluence (green points) and best fits for both VPI models. c) Experimental PL emission FWHM versus pump fluence (green points). The dash-dotted vertical lines in (b) and (c) mark the position of the computed ASE thresholds. d) Losses coefficient $\alpha$ spectrum (black line) and gross gain $\gamma$ spectra (at 1.5 mJ cm$^{-2}$) obtained from both VPI models. For comparison purposes, we have included as well the stimulated emission cross-section spectrum $F/\lambda^4$ in arbitrary units (gray line). e) Net optical gain $g$ versus pump fluence inferred from both VPI models. f) Proportionality factor $\Omega\eta$ versus pump fluence retrieved from both VPI models. For the VPI 2 one, filled and hollow points correspond to ASE and fluorescence, respectively. The stripe length for the VPI experiment was $L = 0.45$ cm.

The inclusion in the model of a non-amplified fluorescence background has important effects on the values of the ASE threshold and of the optical gain. The calculated ASE threshold (vertical dash-dotted lines in Figure 3b,c) yielded by VPI 2 is smaller than that by VPI 1 (0.70 vs. 0.88 mJ cm$^{-2}$). This difference can be understood recalling that, as described in the Experimental Section, the threshold is computed from the evolution of the pure ASE term as a function of the pump fluence. Considering that for VPI 2 the fluorescence background contribution is removed from the threshold calculation, this model allows getting evidence of the appearance of ASE at a lower fluence than in VPI 1, overall when the background contribution is important.

We have also determined the ASE threshold from the experimental data using the methodology described in a previous paper of our group.[65] The method that better allows determining the onset of the ASE process is the so-called visual method, in which the first evidence of emergence of the ASE band defines the threshold. This method leads to a threshold value of 0.86 mJ cm$^{-2}$. Alternatively, in the $I_{peak}$ method, that allows the determination of the excitation regime in which ASE becomes the dominant emission process, the threshold is the value coming from the slope variation in the intensity growth with the excitation fluence. This method yields an ASE threshold of (0.975 ± 0.037) mJ cm$^{-2}$. These values are basically comparable, within about 15%, with the values calculated with methods VPI 2 and VPI 1, respectively. This coincidence evidences the reliability of the calculated values and confirms that VPI 2 is more suitable to determine the excitation regime of the ASE onset, while VPI 1 allows to determine the excitation regime at which ASE becomes dominant over the non-amplified emission.

We further observe that, attending to the rules governing the ASE amplification process, a lower threshold is usually linked to a higher optical gain. Indeed, we show in Figure 3d that the gross optical gain $\gamma$ retrieved by VPI 2 at the peak ASE wavelength is larger than that by VPI 1. Given that the optical losses $\alpha$ (black line) yielded by both methods are the same ($\alpha = 1.06 \pm 0.01$ cm$^{-1}$ at 531 nm), then the net optical gain $g$ should be larger for VPI 2. This is confirmed in Figure 3e, where we plot the optical gain $g$ as a function of the pump fluence, as retrieved by methods VPI 1 and VPI 2. This difference evidences that the presence of the background fluorescence signal has also important consequences on the proper net gain determination.

Interestingly, the optical gains obtained previously from the VSL analysis in Figure 2 were as well larger when a background signal was considered for the fit (expression VSL 2), than when only considering one pure ASE signal (expression VSL 1). Actually, both observations are related since, as we explained in the Experimental Section, expression VPI 1 and VPI 2 are generalizations of expressions VSL 1 and VSL 2, respectively. The presence of a linearly growing fluorescence background forces the

minimization algorithm to explore regions with smaller optical gains so that expression VPI 1 can properly fit the experimental data at both large and small pump fluences. At the same time, it is forced to explore regions of larger proportionality factors $\Omega\eta$. This can be clearly seen in Figure 3f, where we represent $\Omega\eta$ obtained by methods VPI 1 and VPI 2 as a function of the pump fluence. The values of $\Omega\eta$ for the pure ASE signal (filled points) are significantly larger for VPI 1 than for VPI 2. In addition, the values of $\Omega\eta$ for the fluorescence background yielded by VPI 2 (hollow points) are almost exactly the same as those obtained for the pure ASE signal in VPI 1. From this analysis we can draw several conclusions: first, these results suggest that VPI 1 is indirectly detecting a strong background fluorescence, even when it is a process not considered in its analytical expression (Equation 6). Unfortunately, one cannot access this hidden information without the use of expression VPI 2. And second, the results in Figure 3f suggest that, in sample NC-DDAB, there is a strong contribution from a background fluorescent signal, a fact that is in full agreement with the results in Figures 2c, and 3a,b. Thus, we can use the values of $\Omega\eta$ rendered by VPI 2 as an indicator of the presence, and magnitude, of the excess background fluorescence.

As a final comment on the net optical gains $g$, we observe that the values obtained in the VSL analysis are significantly larger than those obtained with the VPI analysis. We thoroughly analyzed this behavior in our previous publication,[64] and we can explain it by noting that both VSL 1 and VSL 2 give a sort of "small-signal" gain, while the VPI 1 and VPI 2 yield the "saturated" gain corresponding to the stripe length used for the experiments, which is significantly long for the sample NC-DDAB. Note that the longer the stripe length becomes, the smaller the fitted gain is, as there is a stronger saturation.

To complete the discussion on the VPI analysis, we summarize in Table 1 the applicability conditions and limitations of both VPI methods, as we did with the VSL expressions. In view of these results, the expression VPI 2, Equation (8), stands out as the best analysis method among the ones we have assessed in this work, since it works for any level of saturation in the gain, can detect the presence of two signals, and, at the same time, is intuitive and backed up by a physical model. Implementing the fitting procedure for VPI 2 is not easy but, as we have already done so in the stand-alone graphical user interface *AgL*,[64] it is moderately easy to use, as it only entails a short learning curve. Nevertheless, the expression VPI 2 is not free from caveats. For example, as there are more fitting parameters, it can lead to larger uncertainties in the fitting parameters when compared to VPI 1, as can be seen in Figure 3 and Figures S3 and S4 (Supporting Information). For the same reason, the fit flexibility increases, potentially leading to unrealistic parameters. Thus, as with any other fitting method, the results should not be blindly trusted. Finally, for the particular case of perovskites, both VPI 1 and VPI 2 can fail for the largest pump values, where the assumptions behind Equations (6), (7), and (8) might be violated if, for example, new photophysical effects are activated. For instance, for NC-DDAB some of these effects, including gain saturation combined with inhomogeneous broadening,[50] lead to an increase in the FWHM once a minimum value has been reached (Figure S5, Supporting Information). In such cases, one should remove from the fit those points where the FWHM increases. This is analogous to removing the experimental points with the longest stripe lengths in the VSL 1 and VSL 2 methods when there is gain saturation. Furthermore, expression VPI 2, and VPI 1 for that matter, would lead to incorrect results in the case that there were two emitting species with different fluorescence spectra (for instance excitons and biexcitons) or if there were two ASE signals, as these extremes are not considered by the physical model behind VPI 2. Anyhow, we want to stress that expression VPI 2 can be used to analyze any kind of material as long as it displays both an ASE band and a fluorescence background, and the former does not re-broaden when increasing the pump fluence.

### 2.3. Origin of Shifted ASE Band

So far we have focused on analyzing the different analytical methods to obtain the optical gain from ASE measurements and on assessing which is the best one. During such analysis we have unambiguously shown that the $CsPbBr_3$ NCs samples display two independent contributions to the PL emission, one from a pure and shifted ASE signal, and another one from an excess background fluorescence. However, we have not questioned yet the origin of these two effects. Here, we will address the reason behind the shift in the ASE band with respect to the fluorescent one.

We can exploit the capabilities of the VPI expressions to obtain photophysical information from the ASE measurements. As we showed in a previous publication,[64] the optical gross gain $\gamma$ in Equations (6) and (8) is proportional to the stimulated emission (SE) cross-section, to the ground state absorption (GSA) cross-section, and to the excited state absorption (ESA) cross-section. Whenever the contribution of ESA is not very relevant, the gain spectrum resembles a combination of the two former processes (SE+GSA). By the same reasoning, any deviation from this combination in the VPI expressions results, could indicate the presence of strong ESA.[66] Figure 3d shows the fitted gross gain $\gamma$ spectra yielded by VPI 1 and VPI 2, the losses coefficient $\alpha$ spectrum (which is proportional to the GSA cross-section), and the quantity $F/\lambda^4$, which is proportional to the SE cross-section (see Experimental Section and ref. [64]). As can be clearly seen, the gross gain $\gamma$ obtained by both VPI 1 and VPI 2 is significantly different to the combination of $\alpha$ and $F/\lambda^4$, suggesting that the effects of ESA are non-negligible. More on the contrary, these results point to the presence of a very strong ESA band almost overlapping with the fluorescence window. In this sense, VPI 2 predicts even a negative $\gamma$ in the wavelength range 505–525 nm, indicating that in this region the ESA cross-section is much stronger than the SE one.[66] Notice that such ESA band is detected as well for samples NC1 and NC1-HMDS (Figures S3 and S4, Supporting Information), suggesting that it is not a numerical artifact but, rather, a distinctive spectroscopic feature of $CsPbBr_3$ NCs. In fact, previous works confirm the existence of an ESA band centered at this region in $CsPbBr_3$ NCs samples.[48,67–72]

We can thus conclude that the ASE band is shifted due to a combination of a large overlap between the extinction coefficient $\alpha$ and fluorescence $F$ spectra (black and gray curves in Figure 3d) and a very strong contribution of ESA within the fluorescence window.

### 2.4. Origin of Excess Fluorescence Background

To address the origin of the excess background fluorescence, we will explore in this subsection different processes that can lead to multiple signals.

#### 2.4.1. Differently Polarized Waveguide Modes

A first possible explanation could be related to the polarization dependence of the waveguiding efficiency. It has been long known that the pump polarization affects the emission polarization and properties in ASE and laser devices.[73,74] For transversal pumping and emitting centers (dipoles, actually) mostly fixed at a spatial position and orientation, the trend is clear. If the pump field is polarized along the *y*-axis (Figure 1), the emitters would preferentially couple to the transverse electric (TE) waveguide modes and the emission should be mostly polarized along the *y*-axis. If excited with a polarization along the *x*-axis, the emitters could couple to both the TE and transverse magnetic (TM) waveguide modes and the emission should be mostly depolarized. All this discussion holds if the position and orientation of the emission dipole is fixed. But perovskites are characterized for having a notable charge carrier diffusion,[75,76] meaning that there is a high chance that the orientation and position of the emission dipole moment is randomized before emission. In other words, the emission would be shared between the TE and TM modes, regardless of the pump polarization. The amount going into each mode would ultimately depend on the number of TE and TM modes, on their coupling strength, and on the stimulated emission rate, as the dipole may not have time to be randomized before being stimulated to emit a photon. Accordingly, the presence of both TE and TM modes in emission could somewhat contribute to the excess of spurious fluorescence signal.

To check this hypothesis, we run a polarization-resolved ASE study on sample NC-DDAB. In **Figure** 4a,b we display the PL spectra corresponding to the TE and TM modes when the sample is pumped, respectively, below and above threshold. At a low pump fluence, both polarized modes display almost no difference in the output spectra, other than small changes in intensity coming from pulse to pulse fluctuations. At a high pump fluence, in contrast, the ASE band is much more pronounced for the TE modes than for the TM ones, as the electric field in the former type is more strongly confined to the waveguide, where the light-matter interaction takes place (Table S2, Supporting Information). While these results are obtained for a depolarized laser as pumping source, analogous results are observed when the laser is polarized, either along the *y*- or *x*-axis (results not shown). Attending to the previous discussion, this is indirect evidence of carrier migration and dipole orientation randomization. In any case, the excitation of both polarizations could explain the presence of two signals if a polarizer is not used in detection. This is, the pure ASE signal could come mostly from the TE modes, while the TM emission could be accounting for the background fluorescence. Nevertheless, it is clear from Figure 4b that, even with a polarization-resolved detection, the ASE bands for both modes seem to emerge from a fluorescence background, as happens when no polarizer is used (Figure 3a). In fact, if we repeat the VPI experiment using a polarizer in detection, and apply expression VPI 2, Equation (8), we still detect a significant level of spurious fluorescence. This excess is evidenced when comparing the proportionality factors $\Omega\eta$, that we display in Figure 4c,d for the TE and TM modes, respectively. In particular, when the polarizer is added, $\Omega_2\eta_2 \sim \Omega_1\eta_1$ for both polarizations, meaning that the contribution from the background fluorescence is quite important. Nevertheless, when no polarizer was used, this contribution was significantly larger ($\Omega_2\eta_2 \gg \Omega_1\eta_1$), as can be seen in Figure 3f. These results allow us to conclude that the excitation of TE and TM modes can partially explain the presence of two signals, but it is not the definitive reason.

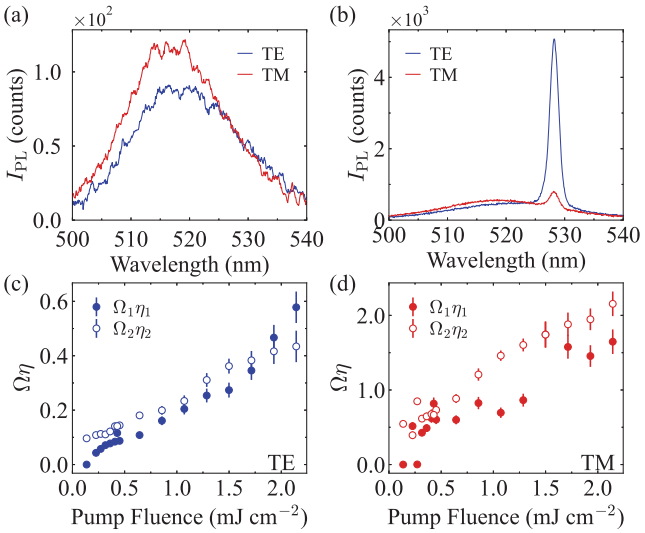


**Figure 4.** Polarization-resolved ASE analysis of sample NC-DDAB: PL spectra for a pump fluence a) below threshold (0.14 mJ cm$^{-2}$) and b) above threshold (2.14 mJ cm$^{-2}$) for the TE (blue curve) and TM (red curve) waveguide modes. Proportionality factor $\Omega\eta$ versus pump fluence retrieved from expression VPI 2 for the c) TE and d) TM modes. Same color code than the previous panels; filled and hollow points correspond to ASE and background fluorescence, respectively. The stripe length for the VPI experiment was $L = 0.45$ cm.

#### 2.4.2. Spatial Inhomogeneities in the Excitation Stripe

An alternative contribution to the presence of two different signals could be a spatial inhomogeneity in the excitation stripe. In most cases, the excitation spot is homogeneous in the longitudinal direction (*x*-axis in Figure 1), but has a Gaussian or bell shape transversal distribution (along the *y*-axis), meaning that the population inversion profile across the excitation spot follows (more or less) the same pattern. At very low pump fluence, the population inversion would remain below the threshold population, and there would only be fluorescence. As the pump fluence increases, the central part of the population inversion profile would eventually cross the threshold, so that ASE would be excited in that region. But in the wings, still below threshold, only fluorescence would be excited. In other words, two different regimes, or signals, would coexist. While enticing, we can mostly rule out this contribution, as the excitation spot is kept fixed across experiments, but each sample shows a different level of background signal, with some of them even lacking it. Notice that this

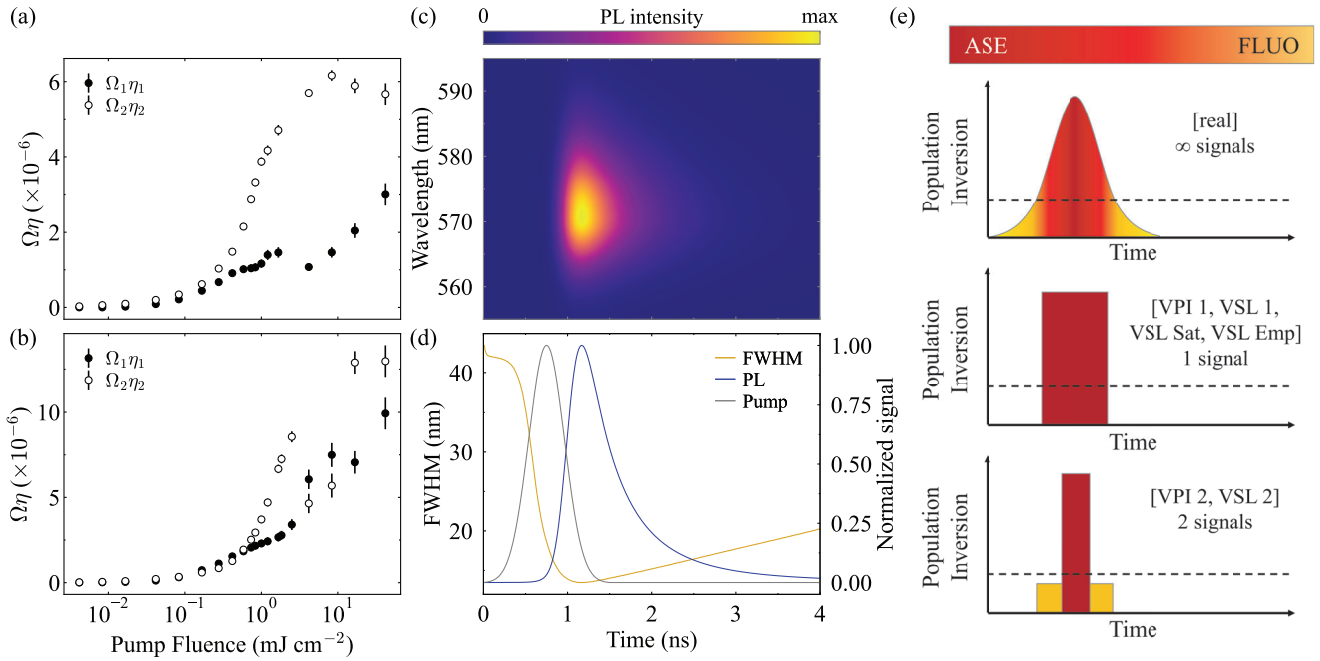


**Figure 5.** Time-domain analysis of the origin of two signals: Proportionality factor $\Omega\eta$ versus pump fluence retrieved from expression VPI 2 for samples a) sim-500ps and b) sim-10ns. Filled and hollow points correspond to ASE and background fluorescence, respectively. c) Heat-map of the time evolution of the PL intensity spectrum for sample sim-500ps excited at a pump fluence of 0.73 mJ cm$^{-2}$. d) Time evolution of the FWHM (left axis, yellow line), and the normalized wavelength-integrated ASE intensity (right axis, blue line), upon excitation with a 0.73 mJ cm$^{-2}$ pump pulse of 500 ps (right axis, gray line). e) Simplified depiction of the time evolution of the available population inversion in a real scenario (top panel), in the single signal approximation (middle panel), and in the two signals approximation (bottom panel). The horizontal dashed line depicts the threshold population inversion.

conclusion holds regardless of the beam width along the *y*-axis, as long as the beam shape is kept fixed. Furthermore, past works have demonstrated the influence on the optical gain calculation of spatial inhomogeneities in the longitudinal direction, like diffraction fringes at the stripe edges[77] or decaying pump intensity due to a not sufficiently expanded beam.[78] Diffraction is not an issue in our VPI experiments, as we are using stripe lengths of 0.45 cm, where the diffraction effects are unimportant.[77] On the other hand, Nitrogen lasers, as the one we have used, emit a nearly top-hat square spot, meaning that the intensity is quite homogenous across it. In any case, we expanded the beam and selected only the central part, ensuring that the pump spot in the sample surfaces was as homogeneous as possible.

### 2.4.3. Time-Domain Effects Due to Pulsed Excitation

A further step in understanding the origin of the background fluorescence signal can be taken by considering the timescales of the pumping and relaxation processes. As with many other problems in Physics, it is best to take a step back and set up a control experiment. In our case, we decided to use spectrally-resolved VPI data from numerical simulations of a polymer thin film doped with a generic dye –lifetime $\tau_f = 6$ ns– (see Experimental Section), in which we assumed a homogeneously broadened single emitting species, a single waveguide mode, no scattering at all, and a perfectly rectangular, homogeneous excitation region.[64] We used simulation results from a dye doped polymer matrix due to a lack of knowledge on the absorption cross-section and emitter density, that are difficult to estimate for a NCs neat film. We anyway underline that this difference is unimportant for our purposes, as we intend to focus on time-domain effects. In particular, we generated sets of VPI data for pump pulse durations shorter and longer than the fluorescence lifetime (samples sim-500ps and sim-10ns, respectively). In principle, the application of expression VPI 2 to these data should result, at most, in a small contribution from a background fluorescence. In contrast, their proportionality factors $\Omega\eta$, that we represent in **Figure** 5a,b, suggest otherwise. In fact, for sample sim-500ps we have $\Omega_2\eta_2 \gg \Omega_1\eta_1$, meaning that the background fluorescence contribution is quite significant. For sample sim-10ns, this contribution is less pronounced, but it is still strong.

Since the only parameter that changes in the simulation of samples sim-500ps and sim-10ns is the pump pulse duration, it is reasonable to postulate a time-domain effect, not captured by the conventional VSL 1 and VPI 1 expressions, as the ultimate responsible for the background fluorescence. We show in Figure 5c the spectro-temporal evolution of a single PL pulse from sample sim-500ps when excited above threshold. To help in the following discussion, we plot in Figure 5d the time evolution of the pump pulse (gray curve), the wavelength-integrated PL signal (blue curve), and the FWHM (yellow curve) corresponding to the PL pulse in Figure 5c. In most experimental cases, the excitation pulse has a temporal bell shape, meaning that the amplification level changes with time. At short times, the pump intensity is low, and the population inversion remains below the threshold population, and there is only fluorescence (weak PL signal and large FWHM). As time advances, the pump increases and the

population inversion reaches a critical limit, leading to the activation of ASE (large PL signal and small FWHM). Notice that the PL signal is delayed with respect to the pump pulse, as the molecules, once excited, remain in the excited state for a finite time, governed by $\tau_f$, before the stimulated emission process begins. In this sense, the shorter the excitation pulse is, the larger the delay becomes. At long times, the pump intensity vanishes, the population inversion is reduced below the threshold value and, eventually, fluorescence is emitted again, with a temporal decay dictated by the fluorescence lifetime. In other words, two different regimes coexist (fluorescence and ASE). It is not a discrete scenario, though, as there is a gradual change of the ASE regime along the duration of the pump pulse, or, rather, during the experimental acquisition time, as we show in Figure 5e (top panel). This is, an infinite number of signals coexist. In contrast, most theoretical treatments of this problem (including the VSL and VPI methods) assume that the population inversion temporal profile is a Heaviside step function (central panel in Figure 5e). In particular, they implicitly perform a time-average of the PL pulse (see ref. [64] for a demonstration), which can be seen as a sort of Continuous Wave (CW) excitation. In this one signal scenario, all the pulse is in the same PL regime, either fluorescence, ASE, or saturated ASE. This first-order approximation (assumed by expressions VSL 1, VSL Sat, VSL Emp, and VPI 1) works good enough in many cases, but in others may not be that good, or it may fail. A second-order approximation, that we illustrate in the bottom panel of Figure 5e, consists of assuming that the population inversion has two different levels along the duration of the pulse, and thus two different signals (ASE plus background fluorescence) are allowed to coexist. Actually, this is the situation captured by models VSL 2 and VPI 2, and that explains why they can fit better to the experimental results.

So, in conclusion, there is not an excess of background fluorescence. On the contrary, it is the expected behavior in a short pulse excitation setting, that is identified as an additional signal due to the simplified, time-averaged, nature of all existing analytical methods. In this sense, if we used a pump pulse much longer than the emitter lifetime (quasi-CW state regime), we would observe that the background fluorescence would become weaker. Actually, we can partially observe this in Figure 5a,b, where the increase of the pulse length diminishes the amount of background fluorescence, as evidenced by the reduction in $\Omega_2\eta_2$ with respect to $\Omega_1\eta_1$. To cross-check that the previous discussion on the time-domain effects is correct, we tried to detect the presence of background fluorescence in experimental data from non-perovskite samples, in which one would not expect this kind of behavior. Remarkably, we have found significant traces of it in a polyfluorene sample[79] (Figure S6, Supporting Information), a Perylene Orange doped PMMA sample[80] (Figure S7, Supporting Information), as well as many other organic semiconductor and dye doped polymer samples.[81–88]

#### 2.4.4. Long-Lived Excitons

The previous discussion helps in deciphering the large excess of background fluorescence observed in $CsPbBr_3$ NCs samples. Specially the results in Figure 5a,b, that show that the shorter the pulse duration becomes –with respect to the fluorescence lifetime–, the stronger the fluorescence background stands. In this sense, $CsPbBr_3$ NCs films display a multiexponential fluorescence decay.[28,44,51,58,89,90] The short lifetime component, on the (sub-)nanosecond scale, has been recently ascribed to a short-range energy migration of localized excitons.[51] On the other hand, the long lifetime component, of the order of tens to hundreds of nanoseconds, can be traced back as well to localized excitons, but delayed by the activation of a long-range diffusion process.[51] The relative weight of each of the contributions –and their impact on the ASE properties– depends on many aspects, including the kind of capping ligand,[17,91,92] the deposition technique,[20,58,60,93–95] the sample post-processing,[89,90] the substrate treatment,[25,94] the ambient temperature and humidity,[26,60,94–96] or the sample aging.[51] Coming back to our problem at hand, the pump pulse duration to study ASE in $CsPbBr_3$ NCs in this work (≈ 3 ns) is longer than the lifetime of the short-lived localized excitons (≈ 0.4 ns[51]). According to the results in Figure 5, the PL signal generated by these localized excitons should contribute moderately to the excess fluorescence (as happened in sample sim-10ns). In contrast, the excitons delayed by the diffusion processes, with a lifetime much longer than the pulse width (≈90 ns[51]), cannot participate in the ASE process, and only provide a fluorescence signal. As this signal accounts for a large percentage of the total emission, the acquired PL spectra display a huge contribution of excess background fluorescence. Actually, Streak camera images of $CsPbBr_3$ NCs samples pumped above threshold back up this idea, as they show an initial fast decay, due to stimulated emission, followed by a slow decay, due to spontaneous emission.[19,28,58] In conclusion, the observed background fluorescence in $CsPbBr_3$ NCs, when using a polarizer in detection, has a twofold origin: an expected contribution due to the non-amplified emission at the beginning and end tails of the short pulse excitation (Figure 5d), and a very strong contribution from spurious fluorescence emitted by long-lived localized states.

## 3. Conclusion

The ultimate goal of this work was to elucidate the origin of the PL properties and spectral signatures of samples based on $CsPbBr_3$ NCs. Specifically, we were trying to answer why the ASE band peak is significantly shifted from the fluorescence maximum and, also, why the former seems to suddenly emerge from, and coexist with, the latter. Given that the ASE characteristics of perovskite waveguides involve different photophysical and photonic processes, finding an adequate methodology to analyze their optical gain is demanded in the first place. An ideal methodology should capture experimental trends like the gain saturation and the background fluorescence, be intuitive and easy to use/implement, and be derivable from a physical model.

In this work, we have carried out a comprehensive assessment, based on these criteria, of the performance of different analytical expressions used in the literature to retrieve the optical gain from ASE experiments, either VSL or VPI. Notice that, while we have performed this analysis on $CsPbBr_3$ NCs films, the conclusions can be generalized to any other kind of gain media. We have shown that most of the proposed models or expressions fail in fulfilling these criteria in full and, hence, one must always ensure that the data chosen for the fitting procedure complies with the assumptions behind the analytical expression. The exception

to this is expression VPI 2, Equation (8), which stands out as the best analysis method among the ones we have assessed in this work, since it works for any level of saturation in the gain, can detect the presence of two signals, and, at the same time, is intuitive and backed up by a physical model.

Leveraging the capabilities of this methodology to analytically assess the experimental ASE measurements, together with the insights provided by time-domain numerical calculations, we can rationalize the ASE behavior in $CsPbBr_3$ perovskite NCs thin films by invoking four distinctive processes: reabsorption, ESA, emission polarization, and long-lived localized excitons. The ASE band is shifted due to a combination of a large overlap between the extinction coefficient $\alpha$ and fluorescence $F$ spectra (black and gray curves in Figure 3d) and a very strong contribution of ESA within the fluorescence window (red curve in Figure 3d). Furthermore, the sense of emergence of the ASE band from the fluorescence one –which is magnified by their detuning– can be explained by an apparent excess of the latter. This excess may have, at the same time, a three-fold origin: the excitation of both TE and TM polarized waveguide modes (Figure 4), each with a different amplification regime; an expected contribution due to the non-amplified emission at the beginning and end tails of the short pulse excitation (Figure 5d); and a strong, yet spurious, fluorescence contributed by long-lived localized excitons.

While this manuscript is focused on $CsPbBr_3$ NCs samples, its conclusions could be readily extrapolated to other kind of perovskites materials, as they commonly show the same PL signatures (ASE band shifted and emerging from the fluorescence band), as well as trap states and multiexponential fluorescence decays.[13,38,39,57,97–102] In fact, to judge by the abundance of these PL trends in literature, it could be an inherent feature of colloidal inorganic semiconducting materials in general (Quantum Dots,[39,55,103,104] or Wells,[39,105–108]) albeit that would need further research for confirmation.

Based on the foregoing, the results in this work establish guidelines to analyze the optical gain, help in understanding the photophysics behind the ASE signatures of both $CsPbBr_3$ NCs and perovskites in general, and provide insightful information on research avenues to increase the efficiency of the light-emitting devices based on these materials.

## 4. Experimental Section

*Samples NC1 and NC1-HMDS*: The NCs were synthesized by adapting the procedure described in ref. [23]. All the details about chemicals and NCs synthesis are reported in the original paper.[25] The NC1 and NC1-HMDS NCs average size is about (9 ± 2) nm. The NC1 solution shows an absorbance spectrum with a clear excitonic peak at 500 nm, a PL spectrum with a peak at 513 nm and PLQY of about 55%.[25] The films were deposited by drop casting 10 µL of the NCs colloidal solution on substrates (NC1 samples) and HMDS functionalized substrates (NC1-HMDS samples). For the functionalization of the substrate: 30 µL of HMDS was drop cast onto the glass substrate and let dry. The adsorbed HMDS was then annealed at 150°C for 30 min and the films cooled down to room temperature for 1 h before NCs solution deposition.[25]

*Sample NC-DDAB*: The NCs were synthesized according to a recently developed approach.[109] Lead bromide ($PbBr_2$, 99.999%), cesium carbonate ($Cs_2CO_3$, 99.9%), diisooctylphosphinic acid (DOPA, 90%), didodecyldimethylammonium bromide (DDAB, 98%), hexane (ReagentPlus, ⩾ 99%), acetone (⩾ 99.5%), toluene (ACS reagent, ⩾99.5%), cyclohexane (ACS reagent, ⩾ 99%) were purchased from Sigma–Aldrich. Trioctylphosphine oxide (TOPO, min. 90%) was purchased from Strem Chemicals. N-octane (⩾ 99%) was purchased from Carl Roth. All chemicals were used as received. $PbBr_2$-TOPO stock solution (0.04 M) was prepared by dissolving $PbBr_2$ (1 mmol, 376 mg) and TOPO (5 mmol, 2.15 g) in octane (5 mL) at 100 °C, followed by dilution with hexane (20 mL) and filtering through a 0.2 µm PTFE filter before use. Cs-DOPA stock solution (0.02 M) was prepared by mixing 100 mg of $Cs_2CO_3$ together with 1 mL of diisooctylphosphinic acid and octane (2 mL) at 100°C followed by dilution with hexane (27 mL) and filtering through a 0.2 µm PTFE filter before use. DDAB stock solution (100 $mgmL^{-1}$, 0.215 M) was prepared by dissolving 300 mg of DDAB in 3 mL anhydrous toluene.

*Synthesis*: In a 25-mL one-neck flask, 2 mL $PbBr_2$-TOPO stock solution was combined along with 3 mL hexane. Under vigorous stirring, 1 mL of Cs-DOPA stock solution was swiftly injected. In 90 s a stock solution of ligands (0.1 mL DDAB in toluene) was added to initiate the ligand exchange on the NC surface. In 1 min after the addition of ligands, the crude solution was concentrated by evaporating hexane on a rotary evaporator down to less than 0.5 mL of residual solvent. The NCs were precipitated from the concentrated colloid by adding non-solvent. NCs were purified using acetone (crude solution:non-solvent 1:1, v/v), followed by solubilization of the obtained NCs in cyclohexane. The concentration of NCs was about 9 $mgmL^{-1}$. The DDAB NCs average size is 8–8.5 nm. The DDAB NCs solution shows an absorbance spectrum with clear excitonic peaks at about 508 and 494 nm and a PL spectrum centered at 513 nm. Near to unity PLQY is reported in literature for DDAB-capped $CsPbBr_3$ NCs solution.[110–113] Thin films were deposited by spin coating (@600rpm) the NCs solution on quartz substrates at room temperature under a chemical fume hood.

*Samples Sim-500ps and Sim-10ns*: Two additional datasets of VPI data were obtained by numerically simulating a conventional experimental scenario: a 1 micron thick polymer film doped with a generic homogeneously broadened dye (lifetime $\tau_f = 6$ ns) is transversally pumped at a wavelength of 532 nm by a laser beam with a Gaussian temporal shape, spatially conformed as a stripe of length $L = 2$ mm and width $b = 150$ µm. The adequate rate equations system was solved for several pump energies with two different pump pulse durations, one shorter than $\tau_f$ ($\tau_p = 500$ ps), and another longer than this ($\tau_p = 10$ ns). These datasets are labelled as samples sim-500ps and sim-10ns, respectively. For the full details about the sample parameters and the system of equations, the reader is referred to the original publication.[64]

*ASE Measurements Set-Up*: ASE measurements were performed by exciting the samples with a LBT MNL100 Nitrogen laser, delivering 3 ns pulses at a wavelength of 337 nm, with a repetition rate of 10 Hz. The pump beam was focused onto the sample surface in a rectangular stripe (4.5 mm length, 80 µm width). The emission was collected from the edge of the sample, dispersed by a 0.75 m focal length spectrograph (Acton 750), and analyzed by an Andor air-cooled Si CCD. The spectral resolution is 0.5 nm. The experiments were carried out at room temperature; in order to limit photodegradation, the PL and gain measurements were performed with the samples under low vacuum ($10^{-1}$ mbar). For the polarization resolved ASE analysis, a WP25M-vis polarizer was used along the detection line.

*Variable Stripe Length (VSL) Method*: The VSL method is a very popular technique to measure the optical gain in active waveguides. In it, the intensity of the edge-emitted PL is measured as a function of the excitation stripe length at a fixed pump intensity. Then, a suitable mathematical expression is fitted to these data to retrieve the optical gain as a fitting parameter. Several expressions can be found that describe the growth of PL intensity ($I_{PL}$) as a function of the stripe length $L$. In this work, the following ones will be analyzed:

a) Expression VSL 1: First reported in ref. [54], it is the most commonly used expression for any type of active material, including perovskites (see ref. [78] and references therein). As such, it is the expression for which the limitations and applicability conditions have been more thoroughly studied.[77,78,114–117] It assumes an unsaturated 1D amplifier in which the

PL emission comes exclusively from ASE. Under these conditions, the growth of ASE intensity $I_{ASE}$ with the stripe length $L$ reads:

$$I_{PL}(L) = I_{ASE}(L) = \frac{A}{g}\left(e^{gL} - 1\right) \quad (1)$$

where $g$ is the net optical gain, and $A$ is a strictly positive proportionality factor that encodes the photophysical properties of the active medium, the level of population inversion, and the excitation geometry.

b) Expression VSL 2: It is an extension of expression VSL 1, to measure $g$ when two emitting species contribute to the emission spectra (excitons and biexcitons in the original publication[55]). Slightly different versions of it have been used for perovskites,[19,56,94] and it reads:

$$I_{PL}(L) = \frac{A_1}{g}\left(e^{gL} - 1\right) + A_2 L \quad (2)$$

where $A_1$ and $A_2$ are analogous to $A$ in Equation (1).

c) Expression VSL Sat: Equations (1) and (2) are valid for stripe lengths in which there is no gain saturation (small-signal regime). For moderate levels of saturation, and only ASE signal, instead, the following expression can be used:[118,119]

$$L = \frac{I_{ASE}(L)/I_s}{g + A/I_s} + \frac{g}{(g + A/I_s)^2} \ln\left|\frac{A + (g + A/I_s) I_{ASE}(L)}{A}\right| \quad (3)$$

where $I_s$ is the saturation intensity. Unlike the previous expressions, Equation (3) is implicit in $I_{ASE}(L)$, and thus must be fitted to a $L$ versus $I_{ASE}(L)$ plot.[119] It has not been used so far in perovskites samples, but it has been utilized for colloidal CdSe nanoplatelets,[107] which have similar ASE signatures.

Notice that Equations (1) and (3) are derived assuming the same physical model, and are solutions, under different approximations (levels of saturation), of the differential equation[119]

$$\frac{dI_{ASE}(x)}{dx} = A + \gamma \frac{I_{ASE}(x)}{1 + I_{ASE}(x)/I_s} - \alpha I_{ASE}(x) \quad (4)$$

where $x$ is the propagation direction, $\gamma$ the gross gain, and $\alpha$ the losses coefficient. Thus, $g = \gamma - \alpha$. For Equation (1), no gain saturation is assumed, or $I_s \to \infty$. For Equation (3), a moderate saturation is considered with $\alpha I_{ASE}(x)/I_s \ll g$.

d) Expression VSL Emp: Introduced in ref. [120] for II-VI semiconductor NCs films, it is an empiric expression to quantify the gain in the presence of saturation. It has been used before for perovskites in some instances,[57,60] and it reads:

$$I_{PL}(L) = I_{ASE}(L) = A e^{g L_s (1 - \exp(-L/L_s))} \quad (5)$$

where $L_s$ is the saturation length.

*Variable Pump Intensity (VPI) Method*: The VPI method is by far the most frequently used technique to analyze the ASE properties in active thin films.[39] In it, the output PL intensity is acquired as a function of the pump excitation value (energy, density, intensity, ...) keeping the stripe length fixed. For the VPI method, there are hardly any analytical expressions that describe the growth of ASE intensity ($I_{ASE}$) as a function of the pump value that can be fitted to the experimental values. In this work, the following expressions are used:

a) Expression VPI 1: It is based on a physical model analogous to the one behind expression VSL 1, Equation (1), but with an explicit dependency on the pump value, generically denoted here as $I_p$. It was first reported in ref. [64], and is given by:

$$I_{PL}(I_p) = I_{ASE}(I_p) = \frac{\Omega \eta F}{\gamma \Delta n - \alpha}\left(e^{(\gamma \Delta n - \alpha)L} - 1\right) \quad (6)$$

$$\Delta n(I_p) = \Delta n_0 \frac{I_p/I^s_{p,1} + (I_p/I^s_{p,2})^m}{1 + I_p/I^s_{p,1} + (I_p/I^s_{p,2})^n} \quad (7)$$

where the pump and wavelength dependencies have been removed from the right-hand side (*rhs*) for notation simplicity. In them, $\eta = \eta(I_p)$ and $\Delta n$ represent different forms of temporally integrated spatially averaged excited state populations, the latter taking into account how well this population and the photon flux overlap in time.[64] $\Delta n_0$ is a normalization factor that ensures that $\Delta n = 1$ at the maximum pump value. $I^s_{p,1}$ and $I^s_{p,2}$ are saturation intensities that, together with the exponents $m$ and $n$ ($m > n$), determine at which pump value, and how fast, the population inversion grows and saturates. $\Omega$ encodes information about the radiative properties of the active medium and the excitation geometry, and $F = F(\lambda)$ is the fluorescence spectrum. Notice that the net optical gain is $g = \gamma \Delta n - \alpha$. For the full details on the formalism, the reader is referred to ref. [64].

b) Expression VPI 2: It is an extension to expression VPI 1 to obtain $g$ when both ASE and a background fluorescence contribute independently to the PL spectra. Newly reported in this work, it reads:

$$I_{PL}(I_p) = \frac{\Omega_1 \eta_1 F}{g}\left(e^{gL} - 1\right) + \frac{\Omega_2 \eta_2 F}{\alpha}\left(1 - e^{-\alpha L}\right) \quad (8)$$

with $g = \gamma \Delta n - \alpha$, and $\Delta n$ given again by Equation (7). The second term at the *rhs* of Equation (8) accounts for fluorescence propagating in the waveguide mode, and is thus subject to losses. Incidentally, at the ASE peak, typically $\alpha L < 1$, and, therefore, a Taylor expansion of the exponential can be performed. Truncating at the first order, and making the substitution $A_i = \Omega_i \eta_i F$, Equation (2) is found. Thus, Equation (8) is a higher-order analogue of Equation (2), but with an explicit dependency on the pump value.

The analytical nature of expression VPI 1 allows computing, instead of visually estimate, the ASE threshold if the adequate threshold criterion is used.[64] For expression VPI 2, the ASE threshold is computed in the same manner, but using only the first term in Equation (8). This is, in this new model, the ASE threshold refers only to the pure ASE contribution, not the PL emission (ASE plus fluorescence background). The fitting procedures for both VPI expressions are implemented in the stand-alone graphical user interface *AgL*,[64] which is freely distributed by the developer (LC) upon request.

## Supporting Information

Supporting Information is available from the Wiley Online Library or from the author.

## Acknowledgements

L.C. acknowledges partial support from a Ramón y Cajal Research Fellowship, Grant RYC2022-038362-I, funded by MCIN/AEI/10.13039/501100011033 and by the European Social Fund Plus (ESF+), and from Grant PID2020-114755GB-C31, funded by MCIN/AEI/10.13039/501100011033. This work was partially funded by the Italian Ministry of University (MUR) under Contract P2022B3W29 (PRIN-PNRR 2022 — LOGIFIB). M. V. Kovalenko from ETH Zürich (Switzerland) and the Laboratory for Thin Films and Photovoltaics, Empa-Swiss Federal Laboratories for Materials Science and Technology, Dübendorf (Switzerland), is acknowledged for providing with the $CsPbBr_3$ nanocrystals used for the realization of the samples investigated in the experiments. We acknowledge support of the publication fee by the CSIC Open Access Publication Support Initiative through its Unit of Information Resources for Research (URICI).

## Conflict of Interest

The authors declare no conflict of interest.

## Data Availability Statement

The data that support the findings of this study are available from the corresponding author upon reasonable request.

## Keywords

amplified spontaneous emission, $CsPbBr_3$, optical gain, perovskite nanocrystals, thin films, variable pump intensity, variable stripe length

Received: April 19, 2024
Revised: June 20, 2024
Published online: July 26, 2024

[1] B. R. Sutherland, E. H. Sargent, *Nat. Photonics* **2016**, *10*, 295.
[2] X. Qi, Y. Zhang, Q. Ou, S. T. Ha, C.-W. Qiu, H. Zhang, Y.-B. Cheng, Q. Xiong, Q. Bao, *Small* **2018**, *14*, 1800682.
[3] J.-P. Correa-Baena, M. Saliba, T. Buonassisi, M. Grätzel, A. Abate, W. Tress, A. Hagfeldt, *Science* **2017**, *358*, 739.
[4] J. Y. Kim, J.-W. Lee, H. S. Jung, H. Shin, N.-G. Park, *Chem. Rev.* **2020**, *120*, 7867.
[5] J. Xu, X. Li, J. Xiong, C. Yuan, S. Semin, T. Rasing, X.-H. Bu, *Adv. Mater.* **2020**, *32*, 1806736.
[6] H. Wang, D. H. Kim, *Chem. Soc. Rev.* **2017**, *46*, 5204.
[7] F. Wang, X. Zou, M. Xu, H. Wang, H. Wang, H. Guo, J. Guo, P. Wang, M. Peng, Z. Wang, Y. Wang, J. Miao, F. Chen, J. Wang, X. Chen, A. Pan, C. Shan, L. Liao, W. Hu, *Adv. Sci.* **2021**, *8*, 2100569.
[8] L. N. Quan, F. P. García de Arquer, R. P. Sabatini, E. H. Sargent, *Adv. Mater.* **2018**, *30*, 1801996.
[9] K. Zhang, N. Zhu, M. Zhang, L. Wang, J. Xing, *J. Mater. Chem. C* **2021**, *9*, 3795.
[10] Y. Mi, Y. Zhong, Q. Zhang, X. Liu, *Adv. Opt. Mater.* **2019**, *7*, 1900544.
[11] L. Lei, Q. Dong, K. Gundogdu, F. So, *Adv. Funct. Mater.* **2021**, *31*, 2010144.
[12] F. Zhao, A. Ren, P. Li, Y. Li, J. Wu, Z. M. Wang, *ACS Nano* **2022**, *16*, 7116.
[13] J. Moon, Y. Mehta, K. Gundogdu, F. So, Q. Gu, *Adv. Mater.* **2023**, *36*, 2211284.
[14] T.-H. Han, K. Y. Jang, Y. Dong, R. H. Friend, E. H. Sargent, T.-W. Lee, *Nat. Rev. Mater.* **2022**, *7*, 757.
[15] M. V. Kovalenko, L. Protesescu, M. I. Bodnarchuk, *Science* **2017**, *358*, 745.
[16] A. Dey, J. Ye, A. De, E. Debroye, S. K. Ha, E. Bladt, A. S. Kshirsagar, Z. Wang, J. Yin, Y. Wang, L. N. Quan, F. Yan, M. Gao, X. Li, J. Shamsi, T. Debnath, M. Cao, M. A. Scheel, S. Kumar, J. A. Steele, M. Gerhard, L. Chouhan, K. Xu, X.-g. Wu, Y. Li, Y. Zhang, A. Dutta, C. Han, I. Vincon, A. L. Rogach, et al., *ACS Nano* **2021**, *15*, 10775.
[17] L. Protesescu, S. Yakunin, M. I. Bodnarchuk, F. Krieg, R. Caputo, C. H. Hendon, R. X. Yang, A. Walsh, M. V. Kovalenko, *Nano Lett.* **2015**, *15*, 3692.
[18] F. Zhang, H. Zhong, C. Chen, X.-g. Wu, X. Hu, H. Huang, J. Han, B. Zou, Y. Dong, *ACS Nano* **2015**, *9*, 4533.
[19] Y. Wang, X. Li, J. Song, L. Xiao, H. Zeng, H. Sun, *Adv. Mater.* **2015**, *27*, 7101.
[20] S. Yakunin, L. Protesescu, F. Krieg, M. I. Bodnarchuk, G. Nedelcu, M. Humer, G. De Luca, M. Fiebig, W. Heiss, M. V. Kovalenko, *Nat. Commun.* **2015**, *6*, 8056.
[21] Y. Shi, R. Li, G. Yin, X. Zhang, X. Yu, B. Meng, Z. Wei, R. Chen, *Adv. Funct. Mater.* **2022**, *32*, 2207206.
[22] M. Athanasiou, A. Manoli, P. Papagiorgis, K. Georgiou, Y. Berezovska, A. Othonos, M. I. Bodnarchuk, M. V. Kovalenko, G. Itskos, *ACS Photonics* **2022**, *9*, 2385.
[23] F. Krieg, S. T. Ochsenbein, S. Yakunin, S. ten Brinck, P. Aellen, A. Süess, B. Clerc, D. Guggisberg, O. Nazarenko, Y. Shynkarenko, S. Kumar, C.-J. Shih, I. Infante, M. V. Kovalenko, *ACS Energy Lett.* **2018**, *3*, 641.
[24] A. Manoli, P. Papagiorgis, M. Sergides, C. Bernasconi, M. Athanasiou, S. Pozov, S. A. Choulis, M. I. Bodnarchuk, M. V. Kovalenko, A. Othonos, G. Itskos, *ACS Appl. Nano Mater.* **2021**, *4*, 5084.
[25] M. L. De Giorgi, F. Krieg, M. V. Kovalenko, M. Anni, *Sci. Rep.* **2019**, *9*, 17964.
[26] A. Balena, A. Perulli, M. Fernandez, M. L. De Giorgi, G. Nedelcu, M. V. Kovalenko, M. Anni, *J. Phys. Chem. C* **2018**, *122*, 5813.
[27] H. Zhang, W. Wen, B. Du, L. Zhou, Y. Chen, S. Feng, C. Zou, L. Wu, H. J. Fan, W. Gao, H. Sun, J. Shang, T. Yu, *Nanoscale Horiz.* **2023**, *8*, 1403.
[28] Y. He, Z. Su, F. Cao, Z. Cao, Y. Liu, C. Zhao, G. Weng, X. Hu, J. Tao, J. Chu, H. Akiyama, S. Chen, *Nanophotonics* **2023**, *12*, 2133.
[29] C. Zhao, J. Tao, J. Tian, G. Weng, H. Liu, Y. Liu, J. Yan, S. Chen, Y. Pan, X. Hu, S. Chen, H. Akiyama, J. Chu, *Chem. Eng. J.* **2021**, *420*, 127660.
[30] C.-Y. Huang, C. Zou, C. Mao, K. L. Corp, Y.-C. Yao, Y.-J. Lee, C. W. Schlenker, A. K. Y. Jen, L. Y. Lin, *ACS Photonics* **2017**, *4*, 2281.
[31] H. Yu, X. Su, Y. Pan, D. Gao, J. Wang, R. Chen, J. Zhang, F. Dou, X. Zhang, K. Ge, X. Shi, T. Zhai, L. Wang, *Opt. Mater.* **2022**, *133*, 112907.
[32] M. Xie, W. Gong, L. Kong, Y. Liu, Y. Mi, H. Guo, S.-N. Luo, *Nanotechnol.* **2021**, *33*, 115204.
[33] D. Yan, T. Shi, Z. Zang, S. Zhao, J. Du, Y. Leng, *Chem. Eng. J.* **2020**, *401*, 126066.
[34] M. B. Price, K. Lewellen, J. Hardy, S. M. Lockwood, C. Zemke-Smith, I. Wagner, M. Gao, J. Grand, K. Chen, J. M. Hodgkiss, E. Le Ru, N. J. L. K. Davis, *J. Phys. Chem. Lett.* **2020**, *11*, 7009.
[35] A. S. Ahmad Kamal, C.-C. Lin, Z. Wang, D. Xing, Y.-C. Lee, M.-H. Chen, Y.-L. Ho, C.-W. Chen, J.-J. Delaunay, *Appl. Phys. Lett.* **2023**, *122*, 071104.
[36] S. Ning, F. Duan, N. Zhang, K. Dai, J. He, Z. Liu, S. Wang, F. Zhang, *Opt. Express* **2023**, *31*, 301.
[37] A. Liu, G. Guan, X. Chai, N. Feng, M. Lu, X. Bai, Y. Zhang, *Laser Photonics Rev.* **2022**, *16*, 2200189.
[38] M. L. De Giorgi, M. Anni, *Appl. Sci.* **2019**, *9*, 4591.
[39] N. Feng, M. Lu, S. Sun, A. Liu, X. Chai, X. Bai, J. Hu, Y. Zhang, *Laser Photonics Rev.* **2023**, *17*, 2200908.
[40] M. Anni, S. Lattante, *Organic Lasers: Fundamentals, Developments, and Applications*, Pan Stanford Publishing, Stanford **2018**.
[41] Y.-S. Park, J. Roh, B. T. Diroll, R. D. Schaller, V. I. Klimov, *Nat. Rev. Mater.* **2021**, *6*, 382.
[42] J. Li, X. Yuan, P. Jing, J. Li, M. Wei, J. Hua, J. Zhao, L. Tian, *RSC Adv.* **2016**, *6*, 78311.
[43] S. M. Lee, C. J. Moon, H. Lim, Y. Lee, M. Y. Choi, J. Bang, *J. Phys. Chem. C* **2017**, *121*, 26054.
[44] N. Yarita, H. Tahara, T. Ihara, T. Kawawaki, R. Sato, M. Saruyama, T. Teranishi, Y. Kanemitsu, *J. Phys. Chem. Lett.* **2017**, *8*, 1413.
[45] P. Geiregat, J. Maes, K. Chen, E. Drijvers, J. De Roo, J. M. Hodgkiss, Z. Hens, *ACS Nano* **2018**, *12*, 10178.
[46] J. A. Castañeda, G. Nagamine, E. Yassitepe, L. G. Bonato, O. Voznyy, S. Hoogland, A. F. Nogueira, E. H. Sargent, C. H. B. Cruz, L. A. Padilha, *ACS Nano* **2016**, *10*, 8603.
[47] Y. Liu, J. Wang, L. Zhang, W. Liu, C. Wu, C. Liu, Z. Wu, L. Xiao, Z. Chen, S. Wang, *Opt. Express* **2019**, *27*, 29124.
[48] W. Zhao, Z. Qin, C. Zhang, G. Wang, X. Huang, B. Li, X. Dai, M. Xiao, *J. Phys. Chem. Lett.* **2019**, *10*, 1251.
[49] Y. Wang, M. Zhi, Y.-Q. Chang, J.-P. Zhang, Y. Chan, *Nano Lett.* **2018**, *18*, 4976.
[50] J. Navarro-Arenas, I. Suárez, V. S. Chirvony, A. F. Gualdrón-Reyes, I. Mora-Seró, J. Martínez-Pastor, *J. Phys. Chem. Lett.* **2019**, *10*, 6389.

[51] A. Cretí, M. Lomascolo, Y. Zhang, M. L. De Giorgi, O. F. Mohammed, M. Anni, *Adv. Opt. Mater.* **2023**, *11*, 2202062.
[52] J. Navarro-Arenas, A. F. Gualdrón-Reyes, V. S. Chirvony, I. Mora-Seró, J. Martínez-Pastor, I. Suárez, in *2020 22nd International Conference on Transparent Optical Networks (ICTON)*, IEEE, Piscataway, NJ **2020**, pp. 1–4.
[53] D. Kim, H. Ryu, S. Y. Lim, K. M. McCall, J. Park, S. Kim, T. J. Kim, J. Kim, Y. S. Kim, M. G. Kanatzidis, H. Cheong, J. I. Jang, *Chem. Mater.* **2021**, *33*, 7185.
[54] K. L. Shaklee, R. F. Leheny, *Appl. Phys. Lett.* **1971**, *18*, 475.
[55] A. V. Malko, A. A. Mikhailovsky, M. A. Petruska, J. A. Hollingsworth, H. Htoon, M. G. Bawendi, V. I. Klimov, *Appl. Phys. Lett.* **2002**, *81*, 1303.
[56] S. M. H. Qaid, H. M. Ghaithan, B. A. Al-Asbahi, A. S. Aldwayyan, *ACS Omega* **2021**, *6*, 5297.
[57] G. Xing, N. Mathews, S. S. Lim, N. Yantara, X. Liu, D. Sabba, M. Grätzel, S. Mhaisalkar, T. C. Sum, *Nat. Mater.* **2014**, *13*, 476.
[58] L. Zhang, F. Yuan, H. Dong, B. Jiao, W. Zhang, X. Hou, S. Wang, Q. Gong, Z. Wu, *ACS Appl. Mater. Interfaces* **2018**, *10*, 40661.
[59] L. Zhu, S. Huang, Y. Liu, R. Li, G. Zhang, Y. Chen, G. Dong, X. Zhang, B. Guan, *Laser Photonics Rev.* **2024**, *n/a*, 2400030.
[60] M. L. De Giorgi, A. Perulli, N. Yantara, P. P. Boix, M. Anni, *J. Phys. Chem. C* **2017**, *121*, 14772.
[61] C.-Y. Yang, L.-Y. Jian, Y.-T. Lee, Z.-L. Tseng, J.-H. Lin, *Sci. Rep.* **2022**, *12*, 10102.
[62] R. Liu, W. Chen, L. Liu, Y. Lu, W. Li, T. Fu, X. Liu, X.-C. Hang, Z. Sun, *Appl. Phys. Lett.* **2021**, *118*, 251106.
[63] D. Wang, R. Q. Liu, X. Tan, Q. Liu, H. R. Nan, S. L. Sang, F. Chen, W. Huang, *Opt. Mater. Express* **2020**, *10*, 981.
[64] L. Cerdán, *Opt. Laser Tech.* **2020**, *121*, 105814.
[65] S. Milanese, M. L. De Giorgi, L. Cerdán, M.-G. La-Placa, N. F. Jamaludin, A. Bruno, H. J. Bolink, M. V. Kovalenko, M. Anni, *Molecules* **2022**, *27*, 4261.
[66] L. Cerdán, M. Anni, M. L. De Giorgi, P. G. Boj, M. A. Díaz-García, *Opt. Laser Tech.* **2021**, *136*, 106766.
[67] X. Liu, J. Han, Y. Li, B. Cao, C. Sun, H. Yin, Y. Shi, M. Jin, C. Liu, M. Sun, D. Ding, *Opt. Express* **2019**, *27*, A995.
[68] Y. Zhang, H. Zhu, T. Huang, Z. Song, S. Ruan, *Photon. Res.* **2019**, *7*, 837.
[69] B. R. C. Vale, E. Socie, A. Burgos-Caminal, J. Bettini, M. A. Schiavon, J.-E. Moser, *J. Phys. Chem. Lett.* **2020**, *11*, 387.
[70] L. Wu, M. Zhang, S. Yang, R. Wu, S. Gong, Q. Han, W. Wu, *J. Alloys Compd.* **2021**, *889*, 161721.
[71] C. Yuan, Y. Wang, X. Shen, B. Chen, F. Hu, L. Chen, Z. Wang, Q. Ouyang, *Opt. Mater.* **2022**, *134*, 113090.
[72] Y. Wu, Z. Huang, Q. Sun, V. D. Ta, S. Wang, Y. Wang, *Laser Photonics Rev.* **2023**, *17*, 2200703.
[73] F. P. Schäfer, *Dye Lasers*, Springer-Verlag, Berlin, Germany **1990**.
[74] I. Gozhyk, M. Boudreau, H. R. Haghighi, N. Djellali, S. Forget, S. Chénais, C. Ulysse, A. Brosseau, R. Pansu, J.-F. Audibert, S. Gauvin, J. Zyss, M. Lebental, *Phys. Rev. B* **2015**, *92*, 214202.
[75] M. Seitz, A. J. Magdaleno, N. Alcázar-Cano, M. Meléndez, S. W. Lubbers, Tim J.and Walraven, S. Pakdel, E. Prada, R. Delgado-Buscalioni, F. Prins, *Nat. Commun.* **2020**, *11*, 2035.
[76] S. Gutiérrez Álvarez, W. Lin, M. Abdellah, J. Meng, K. Žídek, T. Pullerits, K. Zheng, *ACS Appl. Mater. Interfaces* **2021**, *13*, 44742.
[77] L. D. Negro, P. Bettotti, M. Cazzanelli, D. Pacifici, L. Pavesi, *Opt. Commun.* **2004**, *229*, 337.
[78] A. L. Alvarado-Leaños, D. Cortecchia, G. Folpini, A. R. Srimath Kandada, A. Petrozza, *Adv. Opt. Mater.* **2021**, *9*, 2001773.
[79] M. Anni, A. Perulli, G. Monti, *J. Appl. Phys.* **2012**, *111*, 093109.
[80] L. Cerdán, A. Costela, G. Durán-Sampedro, I. García-Moreno, M. Calle, M. Juan-y Seva, J. de Abajo, G. A. Turnbull, *J. Mater. Chem.* **2012**, *22*, 8938.
[81] L. Cerdán, A. Costela, I. García-Moreno, O. García, R. Sastre, *Appl. Phys. B* **2009**, *97*, 73.
[82] L. Cerdán, A. Costela, I. García-Moreno, *Org. Electron.* **2012**, *13*, 1463.
[83] L. Cerdán, A. Costela, G. Durán-Sampedro, I. García-Moreno, *Appl. Phys. B* **2012**, *108*, 839.
[84] L. Cerdán, V. Martínez-Martínez, I. García-Moreno, A. Costela, M. E. Pérez-Ojeda, I. L. Arbeloa, L. Wu, K. Burgess, *Adv. Opt. Mater.* **2013**, *1*, 984.
[85] K. Kazlauskas, G. Kreiza, E. Radiunas, P. Adomėnas, O. Adomėnienė, K. Karpavičius, J. Bucevičius, V. Jankauskas, S. Juršėnas, *Phys. Chem. Chem. Phys.* **2015**, *17*, 12935.
[86] M. Morales-Vidal, P. G. Boj, J. M. Villalvilla, J. A. Quintana, Q. Yan, N.-T. Lin, X. Zhu, N. Ruangsupapichat, J. Casado, H. Tsuji, E. Nakamura, M. A. Díaz-García, *Nat. Commun.* **2015**, *6*, 8458.
[87] M. Alcaire, L. Cerdán, F. L. Zamarro, F. J. Aparicio, J. C. González, F. J. Ferrer, A. Borras, J. P. Espinós, A. Barranco, *ACS Appl. Mater. Interfaces* **2017**, *9*, 8948.
[88] A. Szukalska, A. Szukalski, J. Stachera, D. Zajac, E. Chrzumnicka, T. Martynski, J. Mysliwiec, *Materials* **2022**, *15*, 3.
[89] D. A. Tatarinov, S. S. Anoshkin, I. A. Tsibizov, V. Sheremet, F. Isik, A. Y. Zhizhchenko, A. B. Cherepakhin, A. A. Kuchmizhak, A. P. Pushkarev, H. V. Demir, S. V. Makarov, *Adv. Opt. Mater.* **2023**, *11*, 2202407.
[90] R. A. Rajan, X. Ma, D. Li, Z. Shi, W. Yu, J. Yang, *ACS Photonics* **2023**, *10*, 3255.
[91] D. Yan, T. Shi, Z. Zang, T. Zhou, Z. Liu, Z. Zhang, J. Du, Y. Leng, X. Tang, *Small* **2019**, *15*, 1901173.
[92] Q. Xiong, S. Huang, J. Du, X. Tang, F. Zeng, Z. Liu, Z. Zhang, T. Shi, J. Yang, D. Wu, H. Lin, Z. Luo, Y. Leng, *Adv. Opt. Mater.* **2020**, *8*, 2000977.
[93] Y. Zhong, K. Liao, W. Du, J. Zhu, Q. Shang, F. Zhou, X. Wu, X. Sui, J. Shi, S. Yue, Q. Wang, Y. Zhang, Q. Zhang, X. Hu, X. Liu, *ACS Nano* **2020**, *14*, 15605.
[94] I. Kim, G. E. Choi, M. Mei, M. W. Kim, M. Kim, Y. W. Kwon, T.-I. Jeong, S. Kim, S. W. Hong, K. Kyhm, R. A. Taylor, *Light Sci. Appl.* **2023**, *12*, 285.
[95] G. Morello, S. Milanese, M. L. De Giorgi, N. Calisi, S. Caporali, F. Biccari, N. Falsini, A. Vinattieri, M. Anni, *Nanomaterials* **2023**, *13*, 306.
[96] S. Milanese, G. Morello, M. L. De Giorgi, A. Cretì, H. Andrusiv, M. I. Bodnarchuk, A. Qualtieri, M. Lomascolo, M. V. Kovalenko, M. Anni, *Mater. Today Phys.* **2023**, *35*, 101098.
[97] M. Li, Q. Gao, P. Liu, Q. Liao, H. Zhang, J. Yao, W. Hu, Y. Wu, H. Fu, *Adv. Funct. Mater.* **2018**, *28*, 1707006.
[98] P. Brenner, O. Bar-On, M. Jakoby, I. Allegro, B. S. Richards, U. W. Paetzold, I. A. Howard, J. Scheuer, U. Lemmer, *Nat. Commun.* **2019**, *10*, 988.
[99] V. S. Chirvony, K. S. Sekerbayev, H. Pashaei Adl, I. Suárez, Y. T. Taurbayev, A. F. Gualdrón-Reyes, I. Mora-Seró, J. P. Martínez-Pastor, *J. Lumin.* **2020**, *221*, 117092.
[100] Y. Li, I. Allegro, M. Kaiser, A. J. Malla, B. S. Richards, U. Lemmer, U. W. Paetzold, I. A. Howard, *Mater. Today* **2021**, *49*, 35.
[101] M. L. De Giorgi, A. Cretì, M.-G. La-Placa, P. P. Boix, H. J. Bolink, M. Lomascolo, M. Anni, *Nanoscale* **2021**, *13*, 8893.
[102] K. Wang, C. Huang, Q. Ruan, Y. Zhou, Y. Chen, H. Liu, S. Xiao, Q. Song, *ACS Photonics* **2023**, *10*, 2091.
[103] C. Dang, J. Lee, C. Breen, J. S. Steckel, S. Coe-Sullivan, A. Nurmikko, *Nat. Nanotechnol* **2012**, *7*, 335.
[104] G. L. Whitworth, M. Dalmases, N. Taghipour, G. Konstantatos, *Nat. Photononics* **2021**, *15*, 738.
[105] C. She, I. Fedin, D. S. Dolzhnikov, A. Demortière, R. D. Schaller, M. Pelton, D. V. Talapin, *Nano Lett.* **2014**, *14*, 2772.

[106] B. Guzelturk, Y. Kelestemur, M. Olutas, S. Delikanli, H. V. Demir, *ACS Nano* **2014**, *8*, 6599.
[107] B. Guzelturk, M. Pelton, M. Olutas, H. V. Demir, *Nano Lett.* **2019**, *19*, 277.
[108] Y. Kelestemur, Y. Shynkarenko, M. Anni, S. Yakunin, M. L. De Giorgi, M. V. Kovalenko, *ACS Nano* **2019**, *13*, 13899.
[109] Q. A. Akkerman, T. P. T. Nguyen, S. C. Boehme, F. Montanarella, D. N. Dirin, P. Wechsler, F. Beiglböck, G. Rainò, R. Erni, C. Katan, J. Even, M. V. Kovalenko, *Science* **2022**, *377*, 1406.
[110] J. Dai, H. Roshan, M. De Franco, L. Goldoni, F. De Boni, J. Xi, F. Yuan, H. Dong, Z. Wu, F. Di Stasio, L. Manna, *ACS Appl. Mater. Interfaces* **2024**, *16*, 11627.
[111] M. I. Bodnarchuk, S. C. Boehme, S. ten Brinck, C. Bernasconi, Y. Shynkarenko, F. Krieg, R. Widmer, B. Aeschlimann, D. Günther, M. V. Kovalenko, I. Infante, *ACS Energy Lett.* **2019**, *4*, 63.
[112] H. Wu, Y. Zhang, M. Lu, X. Zhang, C. Sun, T. Zhang, V. L. Colvin, W. W. Yu, *Nanoscale* **2018**, *10*, 4173.
[113] J. Song, J. Li, L. Xu, J. Li, F. Zhang, B. Han, Q. Shan, H. Zeng, *Adv. Mater.* **2018**, *30*, 1800764.
[114] J. Valenta, I. Pelant, J. Linnros, *Appl. Phys. Lett.* **2002**, *81*, 1396.
[115] C. Lange, M. Schwalm, B. Metzger, S. Chatterjee, *J. Appl. Phys.* **2010**, *108*, 103119.
[116] L. Cerdán, *Opt. Lett.* **2017**, *42*, 5258.
[117] H. Wilke, N. M. Hoinka, T. Kusserow, T. Fuhrmann-Lieker, H. Hillmer, *Appl. Phys. Lett.* **2019**, *115*, 173301.
[118] A. Costela, O. García, L. Cerdán, I. García-Moreno, R. Sastre, *Opt. Express* **2008**, *16*, 7023.
[119] L. Cerdán, A. Costela, I. García-Moreno, *J. Opt. Soc. Am. B* **2010**, *27*, 1874.
[120] Y. Chan, J. S. Steckel, P. T. Snee, J.-M. Caruge, J. M. Hodgkiss, D. G. Nocera, M. G. Bawendi, *Appl. Phys. Lett.* **2005**, *86*, 073102.